Front. Phys. 13(3), 138111 (2018)
https://doi.org/10.1007/s11467-018-0755-5

RESEARCH ARTICLE

Self-folding mechanics of graphene tearing and peeling from a substrate

Ze-Zhou He, Yin-Bo Zhu, Heng-An Wu†

CAS Key Laboratory of Mechanical Behavior and Design of Materials, Department of Modern Mechanics, University of Science and Technology of China, Hefei 230027, China
Corresponding author. E-mail: †*wuha@ustc.edu.cn*
Received January 26, 2018; accepted March 3, 2018

Understanding the underlying mechanism in the tearing and peeling processes of graphene is crucial for the further hierarchical design of origami-like folding and kirigami-like cutting of graphene. However, the complex effects among bending moduli, adhesion, interlayer interaction, and local crystal structure during origami-like folding and kirigami-like cutting remain unclear, resulting in challenges to the practical applications of existing theoretical and experimental findings as well as to potential manipulations of graphene in metamaterials and nanodevices. Toward this end, classical molecular dynamics (MD) simulations are performed with synergetic theoretical analysis to explore the tearing and peeling of self-folded graphene from a substrate driven by external force and by thermal activation. It is found that the elastic energy localized at the small folding ridge plays a significant role in the crack trajectory. Due to the extremely small bending modulus of monolayer graphene, its taper angle when pulled by an external force follows a scaling law distinct from that in case of bilayer graphene. With the increase in the initial width of the folding ridge, the self-folded graphene, motivated by thermal fluctuations, can be self-assembled by spontaneous self-tearing and peeling from a substrate. Simultaneously, the scaling law between the taper angle and adhesive energy is independent of the motivations for thermal activation-induced self-assembly and external force tearing, providing effective insights into the underlying physics for graphene-based origami-like folding and kirigami-like cutting.

Keywords graphene, tearing, self-assembly, elastic energy, molecular dynamics simulation

PACS numbers 81.05.ue, 62.25.Mn, 64.75.Yz, 83.10.Rs

1 Introduction

Graphene [1] is a multifunctional two-dimensional (2D) material, which not only possesses extraordinary electrical, thermal and mechanical properties with extensive applications involving composites, nano-electronics, and desalination [2–9], but also is often selected as a model material for fundamental research [10–16]. Owing to its atomic scale thickness and high Föppl–von Kármán number (the ratio between in-plane stiffness and out-of-plane stiffness), graphene can be easily folded with an exceptionally small radius of curvature under external stimuli such as capillary forces, residual stresses and active materials [7, 17–21]. Recently, it has been demonstrated that graphene with kirigami-inspired patterns can be assembled into 3D configurations under in-plane or out-of-plane loading [18, 22], which greatly expands the potential applications of graphene and related 2D materials, to include the fabrication of environment-responsive metamaterials and graphene quantum dots [18, 22, 23]. More surprisingly, graphene can even self-assemble by spontaneous and self-driven sliding, tearing and peeling from a substrate due to thermal activation, thereby facilitating origami-like folding and kirigami-like cutting processes [17]. Whether self-assembled or driven by external force, graphene tearing is one of the most significant processes during its origami-like folding and kirigami-like cutting.

Although specific effort has been devoted to the understanding of tearing fracture in an elastic thin sheet [24–29], there is still a general lack of studies focused on the tearing of graphene [30]. Moura *et al.* conducted theoretical modeling and molecular dynamics (MD) simulations

*Special Topic: Inorganic Two-Dimensional Nanomaterials (Eds. Changzheng Wu & Xiaojun Wu).

of the tearing of a clamped, free-standing graphene under constant downward force, which suggested that it can be applied to measure the fracture toughness of graphene using tearing deformation [31]. To explore the mechanics of exfoliation of 2D materials, Yang *et al.* studied the edge orientation and distribution of 2D materials obtained by mechanical exfoliation [32], demonstrating that the fracture direction is determined synergistically by the tearing direction and material anisotropy of fracture energy [33]. Inspired by tapered graphene nanoribbons torn from an adhesive substrate, Sen *et al.* found that the taper angle of the torn off graphene nanoribbon depends on the competition between the elastic energy in the graphene sheet and graphene-substrate adhesion energy. For low adhesion energy, bending energy stored in the graphene sheet is dominant, and the sine of the taper angle scales as $\sin\theta \propto \sqrt{\gamma_1}$, where γ_1 is the adhesion strength of graphene sheet to substrate, in agreement with previous experimental observations and theoretical modeling [24, 34]. As adhesion strength increases, the stretching energy in the graphene sheet becomes significant, and the sine of the taper angle scales as $\sin\theta \propto \gamma_1^2$ [34]. Annett *et al.* pointed out that graphene interfacial healing tension overcomes the peeling and tearing resistance respectively, and also reported that inward taper occurs due to a tendency to reduce strain energy in the fold [17]. While the self-assembly of graphene by spontaneous tearing and peeling from a substrate has been investigated recently [17, 35], it remains unclear how the bending moduli and adhesion of the graphene together with local crystal structure impact the tearing process. Besides, it is currently unknown how stimuli such as external force and thermal activation influence the mechanism of graphene tearing. Further clarification is thus needed.

In this study, as an effort to explore the underlying mechanism of the tearing and peeling process of graphene, we carry out classical MD simulations and synergetic theoretical analysis to investigate the tearing and peeling of self-folded graphene from a substrate driven by external force and thermal activation. We firstly study the graphene flap peeled from a substrate under external force. It is found that the taper angle of monolayer graphene follows a distinct scaling law differing from bilayer graphene, which is further discussed by invoking a Griffith-style elastic fracture analysis. It is demonstrated that the bending energy is the dominant contribution to the elastic energy of the system for bilayer graphene, while the elastic energy of monolayer graphene includes bending and stretching energy, which together with the adhesion effect act in a nontrivial way to produce a taper angle following a different scaling law. Based on these analyses, the self-tearing process of graphene driven by thermal activation is subsequently investigated. Our MD simulations and mechanical model reveal that the scaling law between the taper angle and adhesive energy is independent of the motivations for thermal activation-induced self-assembly and external force tearing, thereby providing more validation of and insights about the self-assembly process of multilayered graphene from current MD simulations.

2 Models and methods

In order to investigate the properties of graphene tearing and folding on a substrate, the MD simulations were performed using large-scale atomic/molecular massively parallel simulator (LAMMPS) [36]. The interactions among the carbon atoms in graphene sheet were described by the adaptive intermolecular reactive empirical bond order (AIREBO) potential [37]. To simulate the brittle fracture of graphene, the AIREBO potential was modified by using a cut-off distance $r_{cc} = 1.92$ Å in the switching function, beyond which the C-C bonds break [12, 38]. This modification has been shown to capture well the stress-strain behavior of graphene obtained by first-principles calculations. The interactions between graphene and flat substrate were modeled by a Lennard-Jones (LJ) potential with the cutoff distance of 10.0 Å, LJ parameters $\sigma = 3.0$ Å and ε ranging from 0.0001 to 0.12 eV, corresponding to the adhesion strength (γ_1) of the substrate from 0.004 to 5 J/m^2.

To construct the self-folded graphene, two initial parallel crack notches were created in a single layer graphene sheet adhered to a flat substrate. The edge of the flap was firstly lifted vertically along the z direction, bent back, and displaced along the x direction. Then, the system was relaxed using conjugate gradient energy minimization to ensure that the mechanical folding process reached its equilibrium configuration, resulting in the self-folded graphene shown in Fig. 1(b) [20], which is colored and visualized using the OVITO package [39]. Previous researches demonstrated that free graphene sheet tends to fold along armchair and zigzag directions [40]. Therefore, both two configurations of graphene folding (armchair and zigzag) were chosen. For example, as shown in Fig. 1(a), the graphene is folded aligning to the zigzag (folding angle $\chi = 30°$) direction.

In this work, mechanical responses of graphene tearing under external force were investigated by performing MD simulations at 10 K using a Nosé–Hoover thermostat with a damping time step of 0.1 ps. To reduce the impact of boundaries, the graphene sheet had a width $a = 50$ nm, length $b = 80$ nm, and the initial width of flap $W_0 = 20$ nm, as indicated in Fig. 1(a). Additionally, the boundaries of the graphene sheet were fixed to prevent relative slip between the graphene sheet and

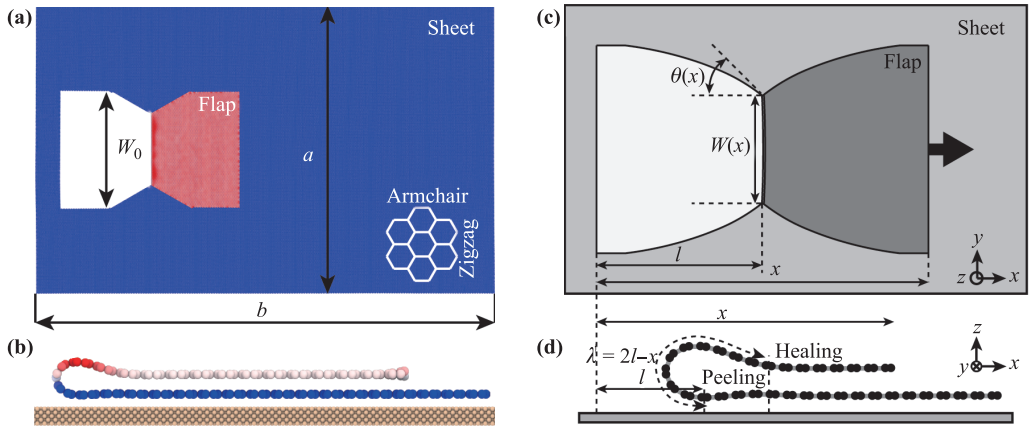

Fig. 1 Schematics of the tearing of graphene. **(a)** Snapshot of tearing monolayer graphene by pulling the flap at a constant velocity along armchair direction. **(b)** The side view of the self-folded monolayer graphene after the energy minimization in MD simulation. **(c, d)** Schematic diagram showing the geometrical parameters involved to describe the tearing process of graphene. The flap sliding direction is indicated by the black arrow. The side view is the cross-section of graphene folding during it peeling and healing on a substrate [17].

substrate. The end of the flap was then moved along the tearing direction at a constant velocity of 1 Å/ps until the flap separated from the sheet. For the process of graphene self-assembly on the substrate, larger graphene sheets were created with initial widths of 160 and 256 nm, which contained 0.9 million and 1.7 million carbon atoms respectively. Then, the folded graphene was relaxed within the canonical (NVT) ensemble at 10 and 300 K for 800 ps to let the system reach its equilibrium configuration. During MD simulations, the models were exposed to free boundary conditions in three dimensions, and substrates were fixed to avoid the impact of substrate deformation.

3 Results and discussion

3.1 Tearing graphene from a substrate

In the first series of MD simulations, self-folded graphene torn from a substrate with the peeling angle equal to π under external force was investigated. In the tearing process, as shown in Fig. 1(a), two crack tips converged to form a tapered tear morphology with the decrease of the width of the folded ridge, which is similar to the tear fracture on an elastic thin sheet in previous experiments and simulations [24, 34]. In addition, there is significant adhesion effect between the graphene sheet and the flap due to the small curvature of the front folded edge. Being different from thin film tearing at macroscale, tearing graphene from a substrate at nanoscale experiences a dynamic self-folded process; that is, schematically showing in Fig. 1(d), the peeling from the substrate and the interfacial healing between two stacked layers of graphene and fracture propagation.

Figures 2(a)–(c) display detailed atomic morphologies of crack edges in torn monolayer graphene for three different scenarios. At low adhesion strength ($\gamma_1 = 0.0043$ J/m^2, $\theta = 24.9°$), the narrowing of the torn graphene ridge is achieved through small surface steps in an armchair orientation that deviate from the tearing direction by 30°, and these alternate with portions of extended propagation in the zigzag direction parallel to peeling direction. Thus, it is the armchair steps that are responsible for the narrowing of the tearing ridge, causing the two crack tips to propagate inward when the taper angle is smaller than 30°, as shown in Fig. 2(a). With the increase of adhesion strength, the lengths of zigzag edge between the armchair steps decrease, resulting in a larger taper angle. At high adhesion strength ($\gamma_1 = 1.25$ J/m^2, $\theta = 46.5°$), the converging is accomplished through another alternate deformation combination, which contains armchair steps and a second zigzag edge orientated at 60° with respect to the peeling direction (first zigzag direction). As indicated in Fig. 2(b), the second zigzag edge dominates the narrowing of the ridge when the taper angle is higher than 30°, and the length of the second surface edge increases rapidly with increasing adhesion strength until the taper angle becomes 60°. For a peeling direction aligned with the armchair direction, however, the surfaces of the torn graphene edge are all along the zigzag surface regardless of adhesion strength, which is similar to self-redirection of tearing edges in graphene [41]. Therefore, the taper angle of graphene torn parallel to the armchair direction is always around 30° as shown in Fig. 2(c).

The crack trajectories and edge geometries of torn bilayer graphene in Figs. 2(d)–(f) show that the deformation and tearing are proceed by different mechanisms

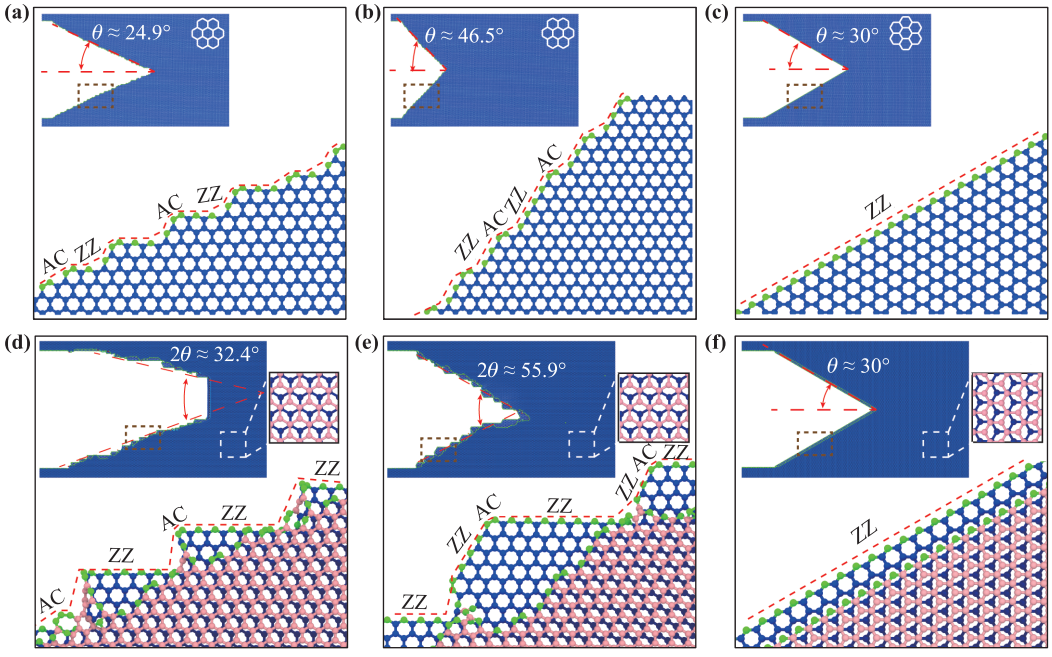

Fig. 2 The tearing shapes and their edge geometries for various adhesion strengths. The edge geometries of zoom areas are signed by brown dashed box. **(a–c)** Tearing results of monolayer graphene for adhesion strength of (a) 4.0E-3, (b) 1.25 J/m^2. **(d–f)** Tearing results of bilayer graphene for adhesion strength of (d) 1.25, (e) 4.18 J/m^2. The upper and lower graphene is colored by magenta and blue respectively. (c) and (f) Graphene torn along armchair direction.

compared with monolayer graphene. First, the tearing edges of bilayer graphene are neither straight nor mirror symmetric, and the upper and lower graphene undergo different forms of deformation. As indicated in Figs. 2(d) and (e), the narrowing of torn bilayer graphene is achieved through big surface steps, which reach the width of 2–3 hexagonal carbon rings and are almost perpendicular to the peeling direction (first zigzag direction). The transition between the two adjoining steps accompanies the formation of new C-C bonds between the upper and lower graphene. At lower adhesion strength ($\gamma_1 = 1.25$ J/m^2), the combination of long first zigzag surface and the big steps dominates the converging of lower graphene, and narrowing of lower graphene at higher adhesion strength ($\gamma_1 = 4.18$ J/m^2) is accomplished through the transition from the long first zigzag surfaces to the second ones, while upper graphene is narrowed via edges similar to those in monolayer graphene as described above. Additionally, comparing Figs. 2(a)–(b) with Figs. 2(c)–(d), we find that the taper angles of bilayer graphene are smaller than those of monolayer graphene tearing, and not sensitive to adhesion strength. These results are in agreement with previous continuum theory, which demonstrates that the taper angle of graphene tearing increases as the bending modulus or the number of layers of graphene increases. The tearing surfaces of bilayer graphene with peeling orientation along the armchair direction, similarly, are all along zigzag surfaces under various adhesion strengths as shown in Fig. 2(f).

To explain the above phenomenon, we focus on the nontrivial tearing trajectories with peeling direction along zigzag direction. Four representative trajectories are presented in Fig. 3(a), in which the width of the tear ridge, W, is plotted as a function of the length torn, l. The sides of the flap torn from single-layer graphene are straight and have the same taper angle θ, but the edges of the flap torn from bilayer graphene are not straight and have many big steps. Thus, an average angle of tearing is utilized by fitting a linear relationship of $W \sim l$ [34]. The results are depicted in Fig. 3(b), where bilayer graphene seems to follow a similar scaling law, $\sin\theta \sim (\gamma_1/\gamma_2)^{1/2}$, where γ_2 is the adhesion energy of the graphene to itself, but monolayer graphene obeys a distinctly different scaling law, $\sin\theta \sim (\gamma_1/\gamma_2)^{0.1}$, which has not been reported before. Following Griffith's theory of fracture analysis, introduced in Refs. [24, 42], we assume that the area of graphene sheet is labeled as A_0 and the area of flap as A_r. The total energy of the system is given by

$$U = U_E + 2\int_0^s G_c t \mathrm{d}\zeta + \gamma_1(A_0 - A_r) + \gamma_2 A_r, \qquad (1)$$

where the first, second, and last two terms are the elastic, fracture and adhesion energies, respectively, t is the graphene thickness, s is the crack length, and G_c is the work of fracture of the graphene.

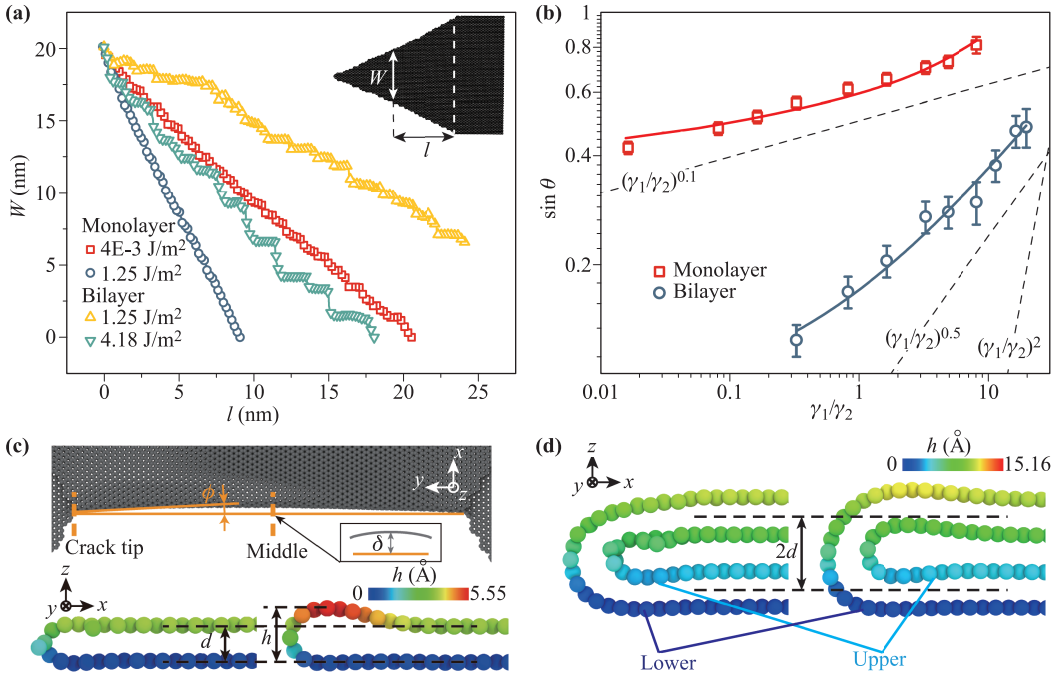

Fig. 3 Deformation mechanisms of graphene tearing. **(a)** Shape of the flap quantized by the width of the ridge W as a function the torn length l. **(b)** The sine of taper angle as a function of the ratio of adhesion strength between graphene to substrate and graphene to itself. The scaling law and theoretical fitting are shown by dashed and solid lines respectively. **(c)** Upper view showing the deformation of the ridge together with the deflection angle ϕ and the sag of the ridge δ. The influence of ϕ is negligible [27]. Side view showing the cross sections of monolayer graphene folding at crack tip and middle of the ridge indicated by orange dashed. **(d)** Cross sections of bilayer graphene folding at crack tip and middle of the ridge indicated by orange dashed lines.

The positions of the crack tips are defined as l and the position of the flap head is denoted as x. The excess of length $\lambda = 2l - x$ is the length of the ridge shown in Figs. 1(c) and (d). The elastic energy of the ridge is a function of its width, W, and its length, λ. Thus, the energy as a function of geometrical parameters is expressed by $U_E = U_E(\lambda = 2l - x, W)$.

The crack tip moves to a position that minimizes the total energy. In a displacement-controlled experiment, the variation of energy is given by

$$\mathrm{d}U = \partial_l U_E \mathrm{d}l + \partial_W U_E \mathrm{d}W + 2G_c t \mathrm{d}s - (\gamma_2 - \gamma_1) W \mathrm{d}l. \quad (2)$$

The requirement yields for energy minimum, $\mathrm{d}U/\mathrm{d}s = 0$, the condition given by

$$\partial_l U_E \cos\theta - 2\partial_W U_E \sin\theta + 2G_c t - (\gamma_2 - \gamma_1) W \cos\theta = 0, \quad (3)$$

where $\mathrm{d}l/\mathrm{d}s = \cos\theta$, $\mathrm{d}W/\mathrm{d}s = -\sin\theta$. Thus, the Griffith's criterion is expressed as

$$G = \frac{1}{2t}[2\partial_W U_E \sin\theta - \partial_l U_E \cos\theta + (\gamma_2 - \gamma_1) W \cos\theta] = G_c. \quad (4)$$

The propagation of the cracks follows the angle θ at which energy release rate is maximal, $\mathrm{d}G/\mathrm{d}\theta = 0$. From Eq. (5), this condition becomes

$$\frac{\mathrm{d}G}{\mathrm{d}\theta} = \frac{1}{2t}[2\partial_W U_E \cos\theta + \partial_l U_E \sin\theta - (\gamma_2 - \gamma_1) W \sin\theta] = 0. \quad (5)$$

In addition, the external force applied to the flap at position x is given by the work theorem as $F = \partial_x U_E$ for a quasi-static fracture propagation. Using the form of elastic energy U_E, the external force can also be formulated as

$$F = \partial_x U_E = -\partial_\lambda U_E = -\frac{1}{2}\partial_l U_E. \quad (6)$$

Combining Eqs. (4), (5), and (6), the equivalent equations for a finite transverse curvature of the ridge are given as follows:

$$F + \frac{1}{2}(\gamma_2 - \gamma_1) W = G_c t \cos\theta, \quad (7)$$

$$\partial_W U_E = G_c t \sin\theta, \quad (8)$$

which correspond to the projections of the forces along the forward and sidewise directions, respectively. Eq. (7)

shows that the external force applied on the end of the flap is balanced by two forces: that of net interface tension [second term of Eq. (7), difference of adhesion strength between peeling and healing] and that of fracture. Additionally, it predicts that the net interface tension force can overcome the tearing resistance when $\gamma_2 > \gamma_1$ and the width of ridge, W, is large enough. Therefore, the interfacial healing, $\gamma_2 W/2$, between graphene sheet and flap can be also regarded as the driving force, F. Equation (8) reveals that inward taper occurs because of a tendency to reduce elastic energy in the folded ridge, equivalent to a force at each crack tip.

To solve Eqs. (7) and (8), it is important and fundamental to estimate the elastic energy, U_E, of the system. In general, it is difficult to completely understand the elasticity in the tearing of a thin film because bending and stretching effects should be considered together with the geometrical non-linearity, but some special cases can be described from an analytical point of view. In the case of tearing of thin film from an adhesive substrate, $F \sim \gamma_1 W \gg G_c t$, the elastic energy of the system stored in the ridge curvature, and is given by $U_E \sim BW\phi^2/\lambda$, where B is the bending modulus of the film, ϕ is the peeling angle, and λ is the length of the ridge [26, 28]. Thus, the taper angle varies linearly with peeling angle and scales as $\sin\theta \sim \sqrt{\gamma_1}$ [34]. In the case of strong adhesion ($\gamma_1 > 8$ J/m^2), stretching energy stored ahead of the tear ridge in the sheet and in the torn flap should be included, and the stretching energy is estimated as $U_S \sim F^2/Et$, resulting in the scaling as $\sin\theta \sim \gamma_1^2$ [34]. These estimations above accord well with the results from experiments and MD simulations.

In our MD simulations, the adhesion strength, γ_1, is smaller than 5 J/m^2 and $Et/G_c t \gg 1$ (inextensible), so the stretching energy is insignificant and the elastic energy is mainly stored in the ridge. To explore the average taper angle of the tearing of bilayer graphene, two layers of graphene can be regarded as a thin film. As shown in Fig. 3(d), the curvature at the crack tips and middle of the ridge is almost the same, so the folded ridge can be regarded as deforming only along its longitudinal direction. The deflection of the folded ridge can therefore be analyzed by the classical elasticity theory of Euler [24], and the elastic energy of the folded bilayer graphene yields $U_E \sim BW/\lambda$. Substituting this expression of elastic energy, U_E, into Eqs. (7) and (8) as well as using the approximation $\cos\theta \simeq 1$ for small angles, we obtain the expression of taper angle

$$\sin\theta = \frac{\alpha}{G_c t}\sqrt{B\gamma_2\left(\frac{\gamma_1}{\gamma_2} - 1 + \frac{2G_c t}{\gamma_2 W}\right)}, \tag{9}$$

where α is a dimensionless constant. For large flaps and adhesion-dominated situations, $\gamma_1 W \gg G_c t$, Eq. (9) is reduced to

$$\sin\theta = \frac{\alpha\sqrt{B\gamma_1}}{G_c t}. \tag{10}$$

This result is similar to the one obtained in Ref. [24]. As shown in Fig. 3(b), the sine of the taper angle is well described by linear fit, $\sin\theta \sim \sqrt{\gamma_1/\gamma_2}$, in agreement with the results of macroscopic continuum theory in previous studies.

However, the sine of the taper angle follows a distinct scaling for the tearing of monolayer graphene. As exhibited in Fig. 3(b), the exponent of scaling of the taper angle for monolayer graphene is about 0.1, obviously smaller than 1/2. Furthermore, the taper angle $\theta \approx 18.4°$, even if the adhesion strength is reduced to zero (see supplementary material Fig. S2), which implies that the elastic energy focused in the ridge is larger than was previously supposed. As indicated in Fig. 3(c), the folded ridge of monolayer graphene deforms not only in the longitudinal direction along its length, but also in the transverse direction along its width. Besides, the curvature at the crack tips is larger than that at the middle of the ridge and almost approaches the limit of graphene bending, which leads to high stress concentration at crack tips, as indicated in Figs. 4(a) and (b). Brau *et al.* [27] supposed that this type of folded ridge possesses the characteristics of a Lobkovsky–Witten ridge, and assumed that the elastic energy of the ridge essentially includes a bending energy, U_B, in the longitudinal direction and a stretching energy, U_S, in the transverse direction in the situation where adhesion is negligible. The bending energy scales as $U_B \sim B\phi^2 W/\lambda$, and the stretching energy $U_S \sim Et\phi^4\lambda^5/W^3$. Upon minimization of the total energy $U_E = U_B + U_S$ with respect

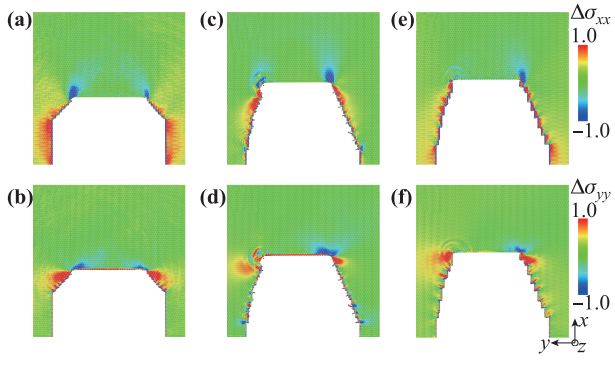

Fig. 4 Virial stress distribution in the graphene sheet for adhesion strength of 0.84 J/m^2. **(a, b)** Tensile stress of monolayer graphene. **(c–f)** Tensile stress of bilayer graphene. (c) and (d) show the stress distribution of the upper graphene. (e) and (f) show the stress distribution of the lower graphene. Compared with bilayer graphene, the stress field of monolayer graphene is symmetric.

Table 1 Structural and mechanical parameters of monolayer and bilayer graphene. The Young's modulus E the thickness t and interfacial adhesion strength γ_2 is calculated by AIREBO potential. Fracture resistances G_c of bilayer graphene are simply set two times that of monolayer graphene.

	E (TPa)	T (Å)	B (eV)	γ_2 (J/m^2)	G_c (J/m^2)	
					$\chi=0°$	$\chi=30°$
Monolayer	1.0 [44]	3.4 [37]	1.4 [48]	0.255	11.7 [12]	11 [12]
Bilayer	1.0 [44]	6.8	35.5 [48]	0.255	23.4	22

to λ ($\partial U_E/\partial\lambda = 0$), we obtain the expression of the elastic energy; $U_E \sim B^2W^5/(Et\lambda^7)$, where E is the in-plane Young's modulus of graphene [27]. In this research, the in-plane Young's modulus for graphene calculated by AIREBO potential is about 1.0 TPa, and the thickness of monolayer graphene is 3.4 Å (see Table 1).

Up to this point, we have not considered the adhesion effect of the substrate on the elastic energy of folded monolayer graphene. As exhibited in Fig. S1, the relationship between the height (h) of the folded ridge and the elastic energy is a function of the adhesion strength of the substrate, and decreases with the increase of adhesion strength. For monolayer graphene, the height and length of the ridge scales $h \sim \lambda$ [27]. Therefore, the elastic energy of monolayer graphene is also a function of adhesion strength, width and length of the ridge, all of which are coupled nonlinearly, so that it is impossible to describe the energy with an analytical formula. To simplify the analysis of elastic energy, we assume that the elastic energy including the adhesion effect can be expressed as $U_E = U_E(\lambda, W, \bar{\gamma})$, where the dimensionless variable $\bar{\gamma} = \gamma_1/\gamma_2$. The elastic energy U_E can be expanded as a Taylor series with respect to

$$U_E(\lambda, W, \bar{\gamma}) = U_E^0(\lambda, W) + \frac{\partial U_E^0}{\partial \bar{\gamma}}\bar{\gamma} + \frac{1}{2}\frac{\partial^2 U_E^0}{\partial \bar{\gamma}^2}\bar{\gamma}^2 + \cdots, \tag{11}$$

where $U_E^0 \sim B^2W^5/Et\lambda^7$. Since the height of the ridge can be given by $h = h(\bar{\gamma})$ by fitting Fig. S1, the first derivative of U_E^0 on $\bar{\gamma}$ can be expressed as

$$\frac{\partial U_E^0}{\partial \bar{\gamma}} = \frac{\partial U_E^0}{\partial \lambda}\frac{\mathrm{d}\lambda}{\mathrm{d}\bar{\gamma}} = \frac{\partial U_E^0}{\partial \lambda}\frac{\mathrm{d}h}{\mathrm{d}\bar{\gamma}}. \tag{12}$$

Neglecting higher order terms, we have

$$U_E(\lambda, W, \bar{\gamma}) \approx U_E^0(\lambda, W)\left(1 - 7\frac{\bar{\gamma}}{h}\frac{\mathrm{d}h}{\mathrm{d}\bar{\gamma}}\right). \tag{13}$$

It is clear that $\mathrm{d}h/\mathrm{d}\bar{\gamma} < 0$, which implies that accounting for the adhesion effect will always increase $U_E(\lambda, W, \bar{\gamma})$. By solving Eqs. (7), (8), and (13) numerically with free parameters of order 1, we find that it predicts the tendency of the taper angle of monolayer graphene indicated in Fig. 3(b) well. This indicates a significant difference between tearing of bilayer graphene and that of single-layer graphene with a peeling angle of π.

Owing to its atomic-scale thickness and small bending modulus, monolayer graphene can be easily folded into extremely small radii of curvature under external stimuli. As shown in Fig. S2, the ridge height of monolayer graphene is smaller than 1 nm, less than the cut-off radius of the adhesion effect, while that of bilayer graphene is greater than 1.4 nm, so the self-folding of single-layer graphene is more influenced by the adhesion strength of the substrate than is bilayer graphene. This also explains why the taper angle of monolayer graphene is extremely sensitive to the adhesion strength of the substrate. Besides, if the bending force, B/h, is low or rupture resistance force G_ct is large, the ridge could bend significantly when it is pulled. In this study, the characteristics of bilayer graphene $B/(G_cth) \approx 1$, while the ratio of monolayer graphene $B/(G_cth) \ll 1$, so the folding ridge of monolayer graphene possesses the characteristics of a Lobkovsky–Witten ridge but this effect can be neglected for the bilayer ridge.

While we have shown the impact of adhesion strength of substrate and thickness of graphene (number of graphene layers) in Fig. 2, several interesting observations deserve further analyses combining the above theoretical analyses. In contrast to monolayer graphene, the two crack trajectories of bilayer graphene appear asymmetric and not straight, and are narrowed through big surface steps and long zigzag edges with large discontinuities. Furthermore, the edges of the upper graphene also differ from those of the lower layer, as exhibited in Figs. 2(d) and (e). To shed light on the trajectory differences between monolayer and bilayer graphene, we will explore the crack path at the atomic scale. For a thin film, the crack path is independent of its past trajectory, for the reason that the elastic energy is localized in a small ridge, so that all the quantities of the crack are functions of inter-crack distance W and $\mathrm{d}W/\mathrm{d}s$ [28]. As shown in Fig. 1(c), since taper angle θ is the local angle between the tangent to the crack trajectory and the x axis, the trajectory can be determined by equation $\mathrm{d}W/\mathrm{d}l = -\tan\theta(W)$ with the initial condition $W(0) = W_0$, demonstrating that the variation in width of the two crack tips only depends on its current value, not on its past [27, 28]. Because it is a case of brittle fracture, crack propagation in monolayer graphene only involves the fracture of C-C bonds, while Sen *et al.* found that at high adhesion strength the transition from the first armchair sections to the second ones is always accompanied by the stress-driven formation of 5–7-defect clusters [34].

Thus, the crack paths of tearing monolayer graphene are similar to those of macroscopic thin film, symmetrical and continuous, but tear edges in Ref. [34] are neither straight nor mirror symmetric at high adhesion strength because of stretching energy ahead of the tear ridge.

However, in the case of tearing of bilayer graphene, there are several differences compared with tearing of monolayer graphene. As indicated in Figs. 2(d) and (e), the upper and lower graphene are AB stacked in the region far away from the crack, while the stacking around the crack deviates from AB stacking, which reveals that there exists evident relative displacement between the two layers of graphene around the crack paths, and that the region around the crack paths also stores elastic energy. Additionally, there are carbons with dangling bonds that form new C-C bonds between the two layers of graphene at big surface steps, leading to stress-activated sheet fracture in these regions exhibited in Figs. 4(c)–(f). These two effects render the crack trajectories of bilayer graphene dependent on their past so that a small disturbance can cause trajectories to become asymmetrical.

A more detailed understanding of the mechanisms can be obtained by considering the deformation difference between the upper and lower graphene layers. As shown in Fig. 3(d), the curvature of the upper graphene layer is much higher than that of the lower, so that the taper angle of the upper layer is larger than that of the lower layer. In other words, the ridge width of the upper graphene diminishes faster than that of the lower. According to the discussion of Figs. 2(a) and (b), the cracks in the upper graphene tend to converge through first armchair and second zigzag edges, while those in the lower graphene are inclined to converge through first zigzag and first armchair edges. Meanwhile, the ridge width of the lower graphene is constrained by that of the upper graphene sheet shown in Fig. 2(d), leading to the formation of C-C bonds during the interaction between the two layers of graphene. The competition of these two effects between upper and lower graphene causes the phenomena shown in Figs. 2(d)–(f). Therefore, interlayer interaction plays an important role in the crack trajectories in bilayer graphene.

3.2 Self-assembly of graphene

As discussed above, the net interface tension force deriving from the difference in the energy release rates of peeling and healing can motivate graphene self-tearing and peeling from a substrate even without external force as $(\gamma_2 - \gamma_1)W/2 > G_c t$. This phenomenon has been studied by Annett *et al.* through theoretical analysis and experiment on a silica substrate, and they showed that thermal activation leads to spontaneous and self-driven sliding, tearing and peeling from a substrate [17]. Neglecting the external force and friction, Eq. (7) can be reduced to [17]

$$\frac{1}{2}\Delta\gamma W = G_c t\cos\theta, \tag{14}$$

where $\Delta\gamma = \gamma_2 - \gamma_1$, is the net interface tension of unit length. Combining Eqs. (8) and (14), it can be seen that the flap growth terminates at a finite width due to its tapering, and flaps with different initial widths should taper and stop with the same final width under similar conditions of temperature, adhesion strength and so on [17].

However, it is unclear how bending moduli, adhesion and local crystal structure impact the tearing process. We now focus on monolayer graphene self-assembly from substrates at various adhesion strengths in the absence of external force by MD simulations. The process of self-assembly involves competition among elastic energy of the folded graphene, the adhesion energy between graphene and substrate, and the graphene-graphene interlayer interaction energy. The graphene flap is first folded by external force, which increases the bending energy of the graphene. After the folded flap is formed, the flap, stimulated by thermal fluctuation, starts to slide on the graphene sheet, and the folding ridge exhibits buckling and gradually produces obvious transverse deformation, as in Fig. 5(a). Then the curved ridge is straightened and shortened because of the crack propagation at its two edges. As the flap and ridge repeat the above movement, the self-assembly of the graphene flap by self-tearing and peeling from a substrate proceeds spontaneously. While the self-assembly occurs at 10 K, it is enhanced by thermal fluctuations at a high temperature ($T = 300$ K), which reduces the strength [43, 44] and accelerates the sliding velocity of the graphene flap (see Movies S1 and S2 in Supplementary material). As shown in Fig. 5(e), the self-assembly processes tend to decrease the energy of graphene, and to stop in a state of energy stability. Varying the adhesion strength of the substrate, we find that the stable energy rises with the increase of adhesion strength, which implies that self-assembly occurs more easily at lower values. Figure 5(f) is the stable state of graphene self-assembly, and shows that the flap is mainly narrowed via first armchair and then zigzag edges, which is similar to the edge tearing of monolayer graphene from a low adherent substrate. In addition, the flap and sheet spontaneously choose AB stacking at the end of the flap, leading to a lower energy state [40].

We detail the evolution of graphene self-assembly at a crack tip in Figs. 5(b)–(d), where the atoms are highlighted by their z coordinate. Because the end of the flap is not subject to an external force and not constrained, there is an obvious stack angle between flap and sheet, which results in Moiré images at overlapping regions [see

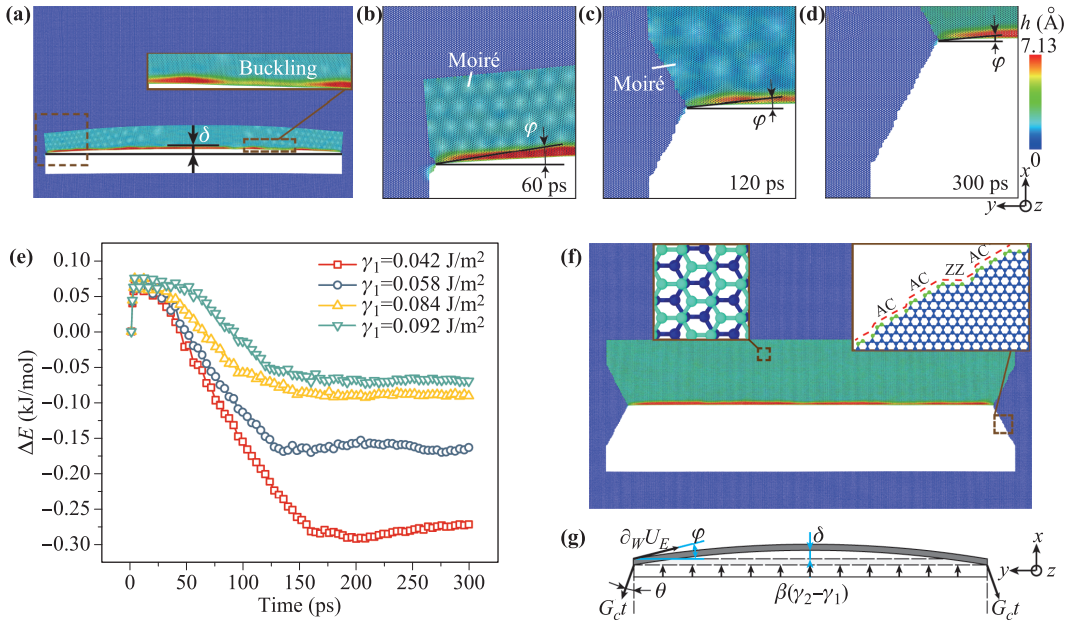

Fig. 5 Formation mechanisms of self-assembly of monolayer graphene. **(a–d)** The evolution of monolayer graphene self-tearing and peeling from a substrate for $T = 10$ K. The crack propagation of zoom area is signed by brown dashed box in (a). **(e)** The change in per-carbon energy during the self-assembly of graphene for $T = 10$ K. **(f)** Upper view and the close up of the final status of graphene after the energy stable for adhesion strength of 0.042 J/m^2. **(g)** Schematic diagram of the balance of forces at the folding ridge.

Figs. 5(b) and (d)]. As the crack propagates, the stack angle becomes small, and the period of the Moiré pattern gradually enlarges until it disappears. When the flap stops sliding, the deflection angle of the ridge at the crack tip becomes constant, as was also observed in Ref. [35]. Therefore, the deflection angle φ plays a significant role during graphene flap self-tearing and peeling from a substrate. This is because in contrast to the tearing of graphene from a substrate with a constant speed as discussed in Section 3.1 (displacement-controlled experiment), the end of the graphene flap here is not constrained, and can freely move along the longitudinal (y axis) or transverse (x axis) direction (see Movie S1 in Supplementary material), which probably causes crack paths to be neither uniform nor symmetrical. Besides, due to thermal disturbance and extremely small bending modulus, the long ridge easily deforms along the transverse direction (x axis). Both of the above reasons lead to the obvious transverse displacement at the middle of the ridge and non-negligible deflection angle at crack tips.

To explain this phenomenon, as shown in Fig. 5(g), the folded ridge can be regarded as a beam, where the sum of fracture resistance $G_c t$ and the derivative $\partial_W U_E$ are the concentrated load at both ends of beam, and the net interface tension $\Delta\gamma W$ is a uniform load on the beam to motivate the ridge deformation and movement. From Fig. 5(a), it is obvious that $\delta/W \ll 1$, so we can estimate $\cos\varphi \simeq 1$ and $\varphi \simeq 4\delta/W$. The sag of the ridge because of the net interfacial tension induces an increase in its length with extensional strain on the order of $(\delta/W)^2$ on an area of size $S \sim \lambda W$, so that the strain energy would yield $U_S \sim Et(\delta/W)^4 S = Et\lambda\delta^4/W^3$ [27], while the work done by the net interfacial tension would follow the scaling law $\omega \sim \beta\Delta\gamma W\delta$. At equilibrium status, the strain energy is equal to the work, $\omega = U_S$. Thus, the deflection angle is given by

$$\sin\varphi \sim \left(\frac{\beta\Delta\gamma W}{Et\lambda}\right)^{1/3}, \tag{15}$$

where β is a dimensionless parameter related to the topology of the folded region shown in Fig. 1(d). Equation (15) implies that the deflection angle φ decreases as the ridge is narrowed, which well explains the reduction of φ in Figs. 5(b)–(d). By considering the balance of forces at the crack tip [45], Eqs. (8) and (14) can be modified as

$$\partial_W U_E \sin\varphi + \frac{1}{2}\beta\Delta\gamma W = G_c t\cos\theta, \tag{16}$$

$$\partial_W U_E \cos\varphi = G_c t\sin\theta. \tag{17}$$

In this way, Eqs. (16) and (17) are coupled together. Analogously, the elastic energy stored in the ridge can be released in two ways: by decreasing its longitudinal curvature or by simply reducing the width of the ridge, which drives the inward tapering of the flap. In the absence of friction, Eqs. (16) and (17) reveal that the flap

growth terminates at a finite width due to its tapering, and its final width and net interfacial tension should be inversely related. Figure 6(a) shows the final width of monolayer graphene self-tearing on a substrate over the adhesion strength range of 0.04–0.17 J/m^2. It demonstrates that the final width is evidently raised with the increase of adhesion strength (decreasing the net interfacial tension), and the final width and adhesion strength are approximately inversely proportional. As the temperature increases ($T = 300$ K), the final widths are reduced as compared to those at lower temperature ($T = 10$ K), because high temperature will accelerate the tearing speed, so that graphene is more easily torn [17]. Moreover, the final width in our MD simulations ranges from 116 nm to 243 nm, while that of monolayer graphene on silica substrate is around 150–230 nm in Ref. [17]. Substituting this value into the fitting curve gives then the adhesion strength of the silica substrate of 0.11–0.2 J/m^2, which is close to previous calculation and experimental results [46, 47].

To further investigate the influence of adhesion, we have measured the taper angle of the above flap after self-assembly stops. As depicted in Fig. 6(b), the taper angle at low temperature ($T = 10$ K) is smaller than that at high temperature. Equation (17) reveals that the taper angle is negatively related to the fracture strength, so that higher temperature increases the taper angle. A further refinement in analysis reveals that the taper angles θ here regardless of temperature exhibit a similar scaling law, close to that of tearing of monolayer graphene under similar conditions as discussed in Section 3.1. This is an interesting and remarkable result, which demonstrates that regardless of external stimuli, such as temperature and external force, as well as size scale (20 nm and hundreds of nanometers), the two dimensionless parameters, $\sin\theta$ and γ_1/γ_2, are consistent characteristics to describe the tendency for convergence of crack trajectories, and their functional relationship mainly depends on the geometry of the folding ridge, as implied by Eqs. (8) and (17). Consequently, although it is unrealistic to perform a full MD simulation of the self-assembly of multilayered graphene, it is possible to predict the tendency for convergence and edges characteristics of crack paths by simulating a small model motivated by external force. Thus, our MD simulations and analysis in Section 3.1 on the crack path can by analogy describe the self-assembly process. As shown in Fig. 3(b), the taper angle of bilayer graphene is 6.3°–9.2° for adhesion strengths of 0.11–0.2 J/m^2, which is consistent with the taper angle $\theta \approx 6°$ in Ref. [17]. This is a good proof of above assumption.

Overall, our MD simulations and analysis provide insights into the underlying physics of the process of self-assembly depicted in Fig. 5. They suggest that the small net interfacial tension can motivate the long folded ridge to move forward with flap self-assembly by self-tearing, self-folding and peeling from a substrate, and the graphene flap could in principle extend to very large scales. Comparing the taper angles in single-layer graphene generated by external force and by self-assembly, we find a consistent characteristic behavior of the sine of the taper angle as a function of the ratio of adhesion strength. This scaling law offers more understanding of the self-assembly process of multilayered graphene from current MD simulations. Furthermore, our MD simulation results exhibited in Fig. 6 also indicate that the self-assembly process could be accommodated via varying the substrate adhesion, number of graphene layers and temperature, in order to achieve controllable origami-like folding and kirigami-like cutting in two-dimensional sheets on a substrate [18].

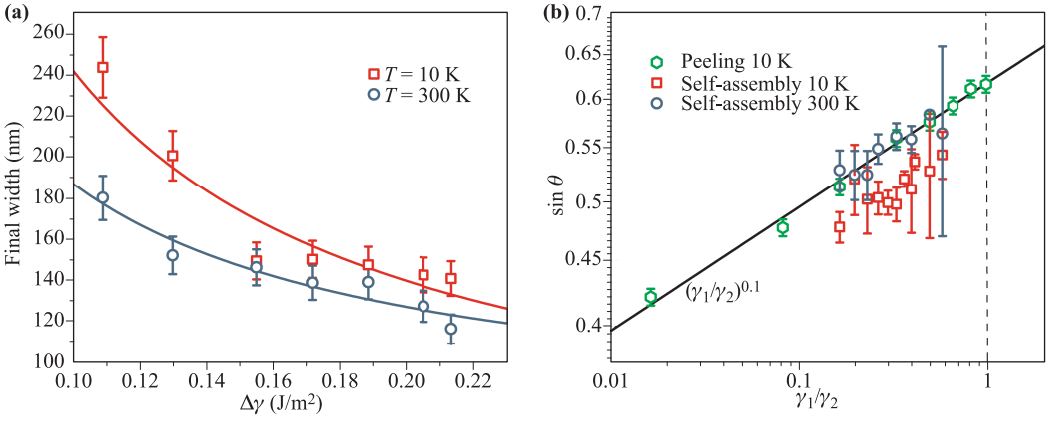

Fig. 6 Geometry of self-assembly graphene. **(a)** Final width of the ridge as a function of interface tension of unit length. The two solid lines are fitting curves by using the functional form $W = A/\Delta\gamma + B$, we obtain $A = 20.44$ J/m, $B = 37.3$ nm for $T = 10$ K, and $A = 12.0$ J/m, $B = 66.9$ nm for $T = 300$ K. **(b)** Comparison of taper angle in self-assembly graphene driven by external force and self-assembled. The scaling law is exhibited by solid line.

4 Conclusion

In summary, we perform MD simulations in conjunction with an analytic model to investigate graphene torn from a substrate through external force and thermal activation. From MD simulations, we find that the tearing of graphene sheets leads to tapered flaps and taper angles are strongly linked to the adhesion strength of the substrate. For bilayer graphene, the taper angle scales as $\sin\theta \sim (\gamma_1/\gamma_2)^{1/2}$, while the monolayer follows a different scaling law, yielding $\sin\theta \sim (\gamma_1/\gamma_2)^{0.1}$. Analytic models reveal that the elastic energy localized over a small region plays a major role in the crack trajectory. The bending energy is the dominant contribution to the elastic energy of the system for bilayer graphene, while the elastic energy of monolayer graphene includes bending and stretching energy, which act together with the adhesion effect in a nontrivial way to produce a taper angle following a different scaling law. In addition, the analytic model indicates that the folded graphene can be torn by self-assembly without external force as long as the net interfacial tension is large enough [see Eq. (14)]. More interestingly, the sine of the taper angle as a function of the adhesion strength is a consistent characteristic regardless of external stimuli and size scale, which provides more validation and insight into the self-assembly process of multilayered graphene from current MD simulations. Nevertheless, MD simulations also demonstrate that the process of self-assembly by self-tearing, self-folding and peeling from a substrate can be controlled by varying the adhesion strength of the substrate, environment temperature and number of graphene layers, giving it potential to be used in origami-like folding and kirigami-like folding of two-dimensional materials.

Electronic supplementary material Supplementary material is available in the online version of this article at https://doi.org/10.1007/s11467-018-0755-5 and is accessible for authorized users.

Acknowledgements This work was jointly supported by the Strategic Priority Research Program of the Chinese Academy of Sciences (Grant No. XDB22040402), the National Natural Science Foundation of China (Grant Nos. 11525211, 11472263, and 11572307), the Anhui Provincial Natural Science Foundation (Grant No. 1808085QA07), and the National Postdoctoral Program for Innovative Talents (Grant No. BX201700225). The authors declare no competing financial interest.

References

1. A. K. Geim and K. S. Novoselov, The rise of graphene, *Nat. Mater.* 6(3), 183 (2007)
2. A. C. Neto, F. Guinea, N. M. Peres, K. S. Novoselov, and A. K. Geim, The electronic properties of graphene, *Rev. Mod. Phys.* 81(1), 109 (2009)
3. R. Nair, H. Wu, P. Jayaram, I. Grigorieva, and A. Geim, Unimpeded permeation of water through helium-leak–tight graphene-based membranes, *Science* 335(6067), 442 (2012)
4. S. Hu, M. Lozada-Hidalgo, F. Wang, A. Mishchenko, F. Schedin, R. Nair, E. Hill, D. Boukhvalov, M. Katsnelson, R. Dryfe, I. V. Grigorieva, H. A. Wu, and A. K. Geim, Proton transport through one-atom-thick crystals, *Nature* 516(7530), 227 (2014)
5. R. Joshi, P. Carbone, F. C. Wang, V. G. Kravets, Y. Su, I. V. Grigorieva, H. Wu, A. K. Geim, and R. R. Nair, Precise and ultrafast molecular sieving through graphene oxide membranes, *Science* 343(6172), 752 (2014)
6. X. Liu, F. Wang, H. Wu, and W. Wang, Strengthening metal nanolaminates under shock compression through dual effect of strong and weak graphene interface, *Appl. Phys. Lett.* 104(23), 231901 (2014)
7. M. Yan, F. Wang, C. Han, X. Ma, X. Xu, Q. An, L. Xu, C. Niu, Y. Zhao, X. Tian, P. Hu, H. Wu, and L. Mai, Nanowire templated semihollow bicontinuous graphene scrolls: Designed construction, mechanism, and enhanced energy storage performance, *J. Am. Chem. Soc.* 135(48), 18176 (2013)
8. D. Akinwande, C. J. Brennan, J. S. Bunch, P. Egberts, J. R. Felts, H. Gao, R. Huang, J. S. Kim, T. Li, Y. Li, K. M. Liechti, N. Lu, H. S. Park, E. J. Reed, P. Wang, B. I. Yakobson, T. Zhang, Y. W. Zhang, Y. Zhou, and Y. Zhu, A review on mechanics and mechanical properties of 2D materials — Graphene and beyond, *Extreme Mechanics Letters* 13, 42 (2017)
9. V. Panchal, C. Giusca, A. Lartsev, R. Yakimova, and O. Kazakova, Local electric field screening in bi-layer graphene devices, *Front. Phys.* 2, 3 (2014)
10. G. Algara-Siller, O. Lehtinen, F. Wang, R. Nair, U. Kaiser, H. Wu, A. Geim, and I. Grigorieva, Square ice in graphene nanocapillaries, *Nature* 519(7544), 443 (2015)
11. Y. Zhu, F. Wang, J. Bai, X. C. Zeng, and H. Wu, Compression limit of two-dimensional water constrained in graphene nanocapillaries, *ACS Nano* 9(12), 12197 (2015)
12. H. Yin, H. J. Qi, F. Fan, T. Zhu, B. Wang, and Y. Wei, Griffith criterion for brittle fracture in graphene, *Nano Lett.* 15(3), 1918 (2015)
13. Z. Song, Y. Ni, and Z. Xu, Geometrical distortion leads to Griffith strength reduction in graphene membranes, *Extreme Mechanics Letters* 14, 31 (2017)
14. J. W. Jiang and H. S. Park, Negative Poisson's ratio in single-layer graphene ribbons, *Nano Lett.* 16(4), 2657 (2016)
15. J. W. Jiang, T. Chang, X. Guo, and H. S. Park, Intrinsic negative Poisson's ratio for single-layer graphene, *Nano Lett.* 16(8), 5286 (2016)

16. G. Wang, Z. Dai, Y. Wang, P. Tan, L. Liu, Z. Xu, Y. Wei, R. Huang, and Z. Zhang, Measuring interlayer shear stress in bilayer graphene, *Phys. Rev. Lett.* 119(3), 036101 (2017)
17. J. Annett and G. L. Cross, Self-assembly of graphene ribbons by spontaneous self-tearing and peeling from a substrate, *Nature* 535(7611), 271 (2016)
18. Y. Zhang, F. Zhang, Z. Yan, Q. Ma, X. Li, Y. Huang, and J. A. Rogers, Printing, folding and assembly methods for forming 3D mesostructures in advanced materials, *Nature Reviews Materials* 2(4), 17019 (2017)
19. X. Meng, M. Li, Z. Kang, X. Zhang, and J. Xiao, Mechanics of self-folding of single-layer graphene, *J. Phys. D Appl. Phys.* 46(5), 055308 (2013)
20. X. Chen, L. Zhang, Y. Zhao, X. Wang, and C. Ke, Graphene folding on flat substrates, *J. Appl. Phys.* 116(16), 164301 (2014)
21. X. Liu, F. Wang, and H. Wu, Anisotropic growth of buckling-driven wrinkles in graphene monolayer, *Nanotechnology* 26(6), 065701 (2015)
22. M. K. Blees, A. W. Barnard, P. A. Rose, S. P. Roberts, K. L. McGill, P. Y. Huang, A. R. Ruyack, J. W. Kevek, B. Kobrin, D. A. Muller, and P. L. McEuen, Graphene kirigami, *Nature* 524(7564), 204 (2015)
23. T. Zhang, S. Wu, R. Yang, and G. Zhang, Graphene: Nanostructure engineering and applications, *Front. Phys.* 12(1), 127206 (2017)
24. E. Hamm, P. Reis, M. LeBlanc, B. Roman, and E. Cerda, Tearing as a test for mechanical characterization of thin adhesive films, *Nat. Mater.* 7(5), 386 (2008)
25. E. Bayart, A. Boudaoud, and M. Adda-Bedia, Finite-distance singularities in the tearing of thin sheets, *Phys. Rev. Lett.* 106(19), 194301 (2011)
26. O. Kruglova, F. Brau, D. Villers, and P. Damman, How geometry controls the tearing of adhesive thin films on curved surfaces, *Phys. Rev. Lett.* 107(16), 164303 (2011)
27. F. Brau, Tearing of thin sheets: cracks interacting through an elastic ridge, *Phys. Rev. E* 90(6), 062406 (2014)
28. B. Roman, Fracture path in brittle thin sheets: a unifying review on tearing, *Int. J. Fract.* 182(2), 209 (2013)
29. A. Ibarra, B. Roman, and F. Melo, The tearing path in a thin anisotropic sheet from two pulling points: Wulff's view, *Soft Matter* 12(27), 5979 (2016)
30. T. Zhang, X. Li, and H. Gao, Fracture of graphene: A review, *Int. J. Fract.* 196(1–2), 1 (2015)
31. M. J. Moura and M. Marder, Tearing of free-standing graphene, *Phys. Rev. E* 88(3), 032405 (2013)
32. Y. Guo, C. Liu, Q. Yin, C. Wei, S. Lin, T. B. Hoffman, Y. Zhao, J. H. Edgar, Q. Chen, S. P. Lau, J. Dai, H. Yao, H. S. Wong, and Y. Chai, Distinctive in-plane cleavage behaviors of two-dimensional layered materials, *ACS Nano* 10(9), 8980 (2016)
33. J. Yang, Y. Wang, Y. Li, H. Gao, Y. Chai, and H. Yao, Edge orientations of mechanically exfoliated anisotropic two-dimensional materials, *J. Mech. Phys. Solids* 112, 157 (2018)
34. D. Sen, K. S. Novoselov, P. M. Reis, and M. J. Buehler, Tearing graphene sheets from adhesive substrates produces tapered nanoribbons, *Small* 6(10), 1108 (2010)
35. A. F. Fonseca and D. S. Galvao, Self-driven graphene tearing and peeling: A fully atomistic molecular dynamics investigation, arXiv: 1801.05354 (2018)
36. S. Plimpton, Fast parallel algorithms for short-range molecular dynamics, *J. Comput. Phys.* 117(1), 1 (1995)
37. S. J. Stuart, A. B. Tutein, and J. A. Harrison, A reactive potential for hydrocarbons with intermolecular interactions, *J. Chem. Phys.* 112(14), 6472 (2000)
38. Y. Wei, J. Wu, H. Yin, X. Shi, R. Yang, and M. Dresselhaus, The nature of strength enhancement and weakening by pentagon-heptagon defects in graphene, *Nat. Mater.* 11(9), 759 (2012)
39. A. Stukowski, Visualization and analysis of atomistic simulation data with OVITO – the open visualization tool, *Model. Simul. Mater. Sci. Eng.* 18(1), 015012 (2010)
40. J. Zhang, J. Xiao, X. Meng, C. Monroe, Y. Huang, and J. M. Zuo, Free folding of suspended graphene sheets by random mechanical stimulation, *Phys. Rev. Lett.* 104(16), 166805 (2010)
41. T. Kawai, S. Okada, Y. Miyamoto, and H. Hiura, Self-redirection of tearing edges in graphene: Tight-binding molecular dynamics simulations, *Phys. Rev. B* 80(3), 033401 (2009)
42. B. Lawn, Fracture of Brittle Solids, Cambridge: Cambridge University Press, 1993
43. Y. Wang and Z. Liu, The fracture toughness of graphene during the tearing process, *Model. Simul. Mater. Sci. Eng.* 24(8), 085002 (2016)
44. Y. Y. Zhang and Y. Gu, Mechanical properties of graphene: Effects of layer number, temperature and isotope, *Comput. Mater. Sci.* 71, 197 (2013)
45. V. Hakim and A. Karma, Laws of crack motion and phase-field models of fracture, *J. Mech. Phys. Solids* 57(2), 342 (2009)
46. S. P. Koenig, N. G. Boddeti, M. L. Dunn, and J. S. Bunch, Ultrastrong adhesion of graphene membranes, *Nat. Nanotechnol.* 6(9), 543 (2011)
47. R. Huang, Graphene: Show of adhesive strength, *Nat. Nanotechnol.* 6(9), 537 (2011)
48. N. Lindahl, D. Midtvedt, J. Svensson, O. A. Nerushev, N. Lindvall, A. Isacsson, and E. E. Campbell, Determination of the bending rigidity of graphene via electrostatic actuation of buckled membranes, *Nano Lett.* 12(7), 3526 (2012)